



Copyright © 2001. Paper 5-001; 0000 Words, 16 Figures, 1 Table.
<http://EarthInteractions.org>

Refinements to SSiB with an Emphasis on Snow Physics: Evaluation and Validation Using GSWP and Valdai Data

David M. Mocko^{*,+} and Y. C. Sud

Laboratory for Atmospheres, NASA Goddard Space Flight Center, Greenbelt,
Maryland

Received 7 June 2000; accepted 6 June 2001

ABSTRACT: Refinements to the snow-physics scheme of the Simplified Simple Biosphere Model (SSiB) are described and evaluated. The upgrades include a partial redesign of the conceptual architecture of snowpack to better simulate the diurnal temperature of the snow surface. For a deep snowpack, there are two separate prognostic temperature snow layers: the top layer responds to diurnal fluctuations in the surface forcing, while the deep layer exhibits a slowly varying response. In addition, the use of a very deep soil temperature and a treatment of snow aging with its influence on snow density is parameterized and evaluated. The upgraded snow scheme produces better timing of snowmelt in Global Soil Wetness Project (GSWP)-style simulations using International Satellite Land Surface Climatology Project (ISLSCP) Initiative I data for 1987–88 in the Russian Wheat Belt region.

To simulate more realistic runoff in regions with high orographic variability, additional improvements are made to SSiB's soil hydrology. These

* Corresponding author address: David M. Mocko, Climate and Radiation Branch, Laboratory for Atmospheres, NASA Goddard Space Flight Center, Code 913, Greenbelt, MD, USA 20771.

E-mail address: mocko@climate.gsfc.nasa.gov

+ Additional affiliation: SAIC/General Sciences Operation, Beltsville, Maryland.

improvements include an orography-based surface runoff scheme as well as interaction with a water table below SSiB's three soil layers. The addition of these parameterizations further helps to simulate more realistic runoff and accompanying prognostic soil moisture fields in the GSWP-style simulations.

In intercomparisons of the performance of the new snow-physics SSiB with its earlier versions using an 18-yr single-site dataset from Valdai, Russia, the revised version of SSiB described in this paper again produces the earliest onset of snowmelt. Soil moisture and deep soil temperatures also compare favorably with observations.

KEYWORDS: Snow and ice; Evapotranspiration; Soil moisture; Runoff and streamflow; Water/energy interactions

1. Introduction and motivation

The Simplified Simple Biosphere Model (SSiB) (Xue et al., 1991) is a biophysical model of land-atmosphere interactions, which was designed to simulate land surface processes in numerical models realistically. The interactions are calculated from the fundamental governing equations (Sellers et al., 1986) and provide fluxes of radiation absorption, reflection, and emission together with momentum, and sensible and latent heat to overlaying atmospheric general circulation models (GCMs) and/or regional models. SSiB has been calibrated for a number of biomes using observational data taken from several regions of the world. In these calibrations and/or evaluations, atmospheric data serve as external forcing, while the model simulates soil/vegetation temperature(s), soil moisture(s), and surface fluxes that are compared with observations. Thus far, validation datasets include the Russian soil moisture data (Robock et al., 1995; Schlosser et al., 1997; Xue et al., 1997), the Hydrological-Atmospheric Pilot Experiment-Mobilhy (HAPEX-Mobilhy) data from France (Xue et al., 1996b), the Cabauw data from the Netherlands (Chen et al., 1997), the Anglo-Brazilian Amazonian Climate Observation Study data (Xue et al., 1996a), the Sahelian Energy Balance Experiment, and HAPEX-Sahel field measurement data from Niger (Xue, 1997). Some evaluations were part of the Project for Intercomparison of Land-surface Parameterization Schemes (PILPS) (Henderson-Sellers et al., 1993), while others were part of the Global Soil Wetness Project (GSWP) (Dirmeyer et al., 1999), which used International Satellite Land Surface Climatology Project (ISLSCP) Initiative I data (Meeson et al., 1995; Sellers et al., 1995). SSiB was included in a National Centers for Environmental Prediction (NCEP) land surface model intercomparison (Chen et al., 1996) using the First ISLSCP Field Experiment data. These evaluations have not only helped to improve SSiB, but also to further understanding the mechanisms of land surface processes in different parts of the world experiencing different climatic conditions, vegetation, and soils. In this way, the ongoing research, development, and evaluation of SSiB has paved the way for more complex interaction studies in a model coupled to a GCM or regional model. SSiB is used within the Goddard Earth Observing System II GCM (Takacs et al., 1994) as well as the Eta Model used by NCEP. Other major institutions using SSiB-based models in an offline mode and/or coupled to a parent atmospheric model

include the Center for Ocean–Land–Atmosphere, Japan Meteorological Agency, and the University of California, Los Angeles.

SSiB, however, had a deficiency in snowmelt timing and meltwater infiltration, first noted by Robock et al. (Robock et al., 1995). Several methods were undertaken to improve the simulation of these processes in SiB-based models (Xue et al., 1997; Sellers et al., 1996). However, when using the global ISLSCP Initiative I data within GSWP, significant snow-physics and meltwater infiltration deficiencies surfaced again (Mocko and Sud, 1998). In fact, the deficiencies were not unique to SSiB. Snow-physics testing and development for models has also been done in several land surface schemes. Among these are Verseghe (Verseghe, 1991), Douville et al. (Douville et al., 1995), Yang et al. (Yang et al., 1997), Loth and Graf (Loth and Graf, 1998a), Liston and Sturm (Liston and Sturm, 1998), Desborough and Pitman (Desborough and Pitman, 1998), Jin et al. (Jin et al., 1999), Sun et al. (Sun et al., 1999), and Smirnova et al. (Smirnova et al., 2000). A summary of the current range of snow-physics packages within land surface schemes is detailed in Slater et al. (Slater et al., 2001). The current design benefited from several ideas and concepts discussed in the above papers and has adapted some of them for use in the revised SSiB model.

Huge deficiencies in snowmelt and meltwater infiltration motivated the development of an earlier snow-physics scheme described in Sud and Mocko (Sud and Mocko, 1999). In that development, the snow layer was separated from the top soil layer. This separation allowed nonreflected shortwave energy to be absorbed in the snow, or to be transmitted through and absorbed in the soil, which had the effect of keeping the soil warm and “blanketed” under the snowpack. Once the snowmelt began, the warmer nonfrozen soil was able to infiltrate the meltwater before the entire snowmelt occurred. Larger meltwater infiltration was accompanied by larger GCM-simulated high northern latitudinal evapotranspiration and precipitation as observed in and around regions of strong seasonal snow cover (Mocko et al., 1999).

The primary motivation for additional improvements was to reduce the remaining biases in the simulation of the onset of snowmelt. Diagnostic tests revealed that the snow surface was not generating the amplitude of diurnal temperature that is observed in the early spring season to initiate midday melting. Consequently, snowpack slowly warmed until the entire snowpack reached the melting temperature at which time it started to melt precipitously. Thus, as compared to observations, there was a delayed initiation of snowmelt, but once it started, it was relatively sudden. This gave the useful clue that deep snowpack needs a diurnal layer, and the only way to achieve this is by separating it from the rest of the pack. Accordingly, a two-layer snow model was designed.

Besides the above, some other deficiencies in SSiB’s hydrology and fluxes also became evident. For instance, SSiB had no provision for generating surface runoff as a function of orography. This motivated the development of an orography/runoff function. Similarly, modifications were needed to improve the sub-surface runoff (or baseflow). An empirical, but reasonable, interaction with the water table was also added. The removal of soil moisture by evaporation or transpiration can now occur from any soil layer, although a weighting function replaces previous formulations. These changes were made to improve both the

simulated soil moisture and runoff as compared to available observations. Finally, skin temperatures were often too high in hot dry regions, which motivated an examination and partial solution of this problem.

The goal of this research and development activity was to further improve the verifiable simulated fields of SSiB, especially with regard to the new snow-physics package. In addition to producing a realistic diurnal cycle of the snowpack, the intended changes were designed to improve the simulation of the snow accumulation and snowmelt timing, meltwater infiltration, and snow surface as well as soil temperatures and runoff. A detailed description of all the improvements to the snow physics in SSiB is found in section 2. The simulated results from all three versions of SSiB (original—Xue et al., 1991; Sud and Mocko, 1999; and that described in this paper) are compared against each other and observations from 1987 to 1988 using the ISLSCP Initiative I data in section 3. The same three model versions are also compared against observations using an 18-yr catchment dataset from Valdai, Russia, in section 4. Conclusions and a discussion are found in section 5.

2. Changes from the one-snow-layer version of SSiB

This section describes the changes made from the one-snow-layer version (OSL) of SSiB (Sud and Mocko, 1999) to the two-snow-layer version (TSL) of SSiB. The first subsection describes additional improvements made to the snow model, while the following two subsections describe other changes related to the model's hydrology and flux calculations. Each improvement was separately evaluated.

2.1 Changes to the snow model

Reduced, yet systematic, delays of snowmelt suggested the need for additional modifications of OSL (Figure 1). The deficiency was due to the inability of OSL to simulate a realistic diurnal temperature. Additionally, a very deep snowpack in the real world would not have a constant temperature over its entire depth, from near the insulated soil–snow interface to the surface, which can radiate and cool freely. Thus a need for introducing a diurnal snow layer was found.

2.1.1 Diurnal snow layer

In the TSL design, the number of prognostic temperature layers is maintained at three. Under a deep snowpack, there is no need for a diurnal soil temperature layer because of the insulating effect of the snow and very little solar input. However, a diurnal snow layer emerges atop the snowpack, which can melt during the day due to strong solar input and can cool significantly at night, much more than the rest of the snow beneath this layer. In this design, when the snow accumulates enough to activate the snow model (currently, the “trigger” is 0.005 m, or 5 mm, water equivalent), the snowpack is divided into two layers that start with the same temperatures, one for the bulk layer T_s and one for the diurnal layer T_{sn} of snow. Over time, these two layers evolve differently through their own energy budget and heat exchange between them. The diurnal layer has a fixed depth of $Z_{sn} = 0.004$ m (4 mm) water equivalent regardless of the total

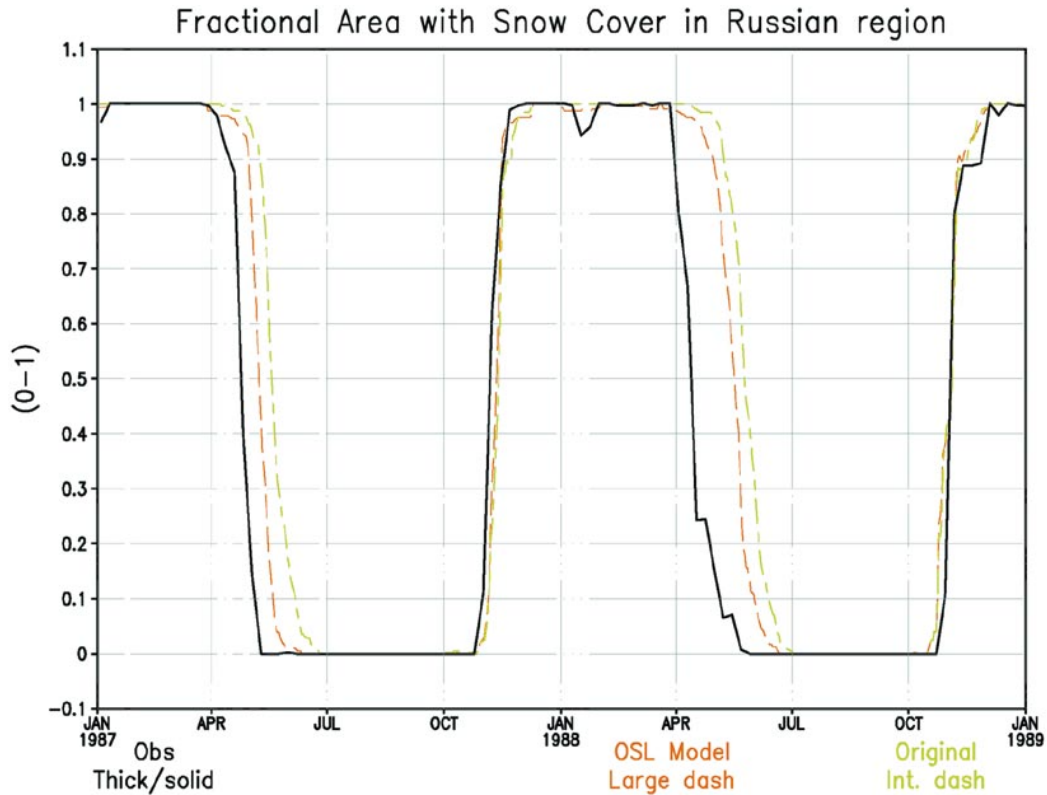


Figure 1. Line plot showing area-averaged snow cover fraction (0-1) in the Russian Wheat Belt region for 1987-88. The long dashed line is from OSL, while the intermittent dashed line is from the original SSiB. The thick solid line is from observations taken from satellite.

depth of snow, and the bulk layer comprises the remainder of the depth of the snowpack. For deep snow, the force-restore layer (Deardorff, 1978) is brought up to work with snow while the two soil layers of temperature are combined into one deep temperature T_d . This feature enables SSiB to operate with the same number of temperature layers. Schematics showing the major design features of OSL and TSL are shown in Figure 2. The configuration of the three soil moisture layers is unchanged between original, OSL, and TSL.

Scientific justifications for moving the diurnal layer atop the snowpack are as follows. This top layer is able to respond to the diurnal changes of the atmosphere if the depth of the diurnal layer is chosen to best respond to these changes. Indeed, the top of the snow can cool radiatively at night, without replenishing all the energy by conduction from the bulk layer. Thus the diurnal layer works as an insulator for the bulk layer. The opposite holds for warm days, particularly with the midday sun in the early spring. These warm days can produce snowmelt in late winter/early spring, which was lacking in OSL. The prognostic equations for TSL are discussed in the appendix.

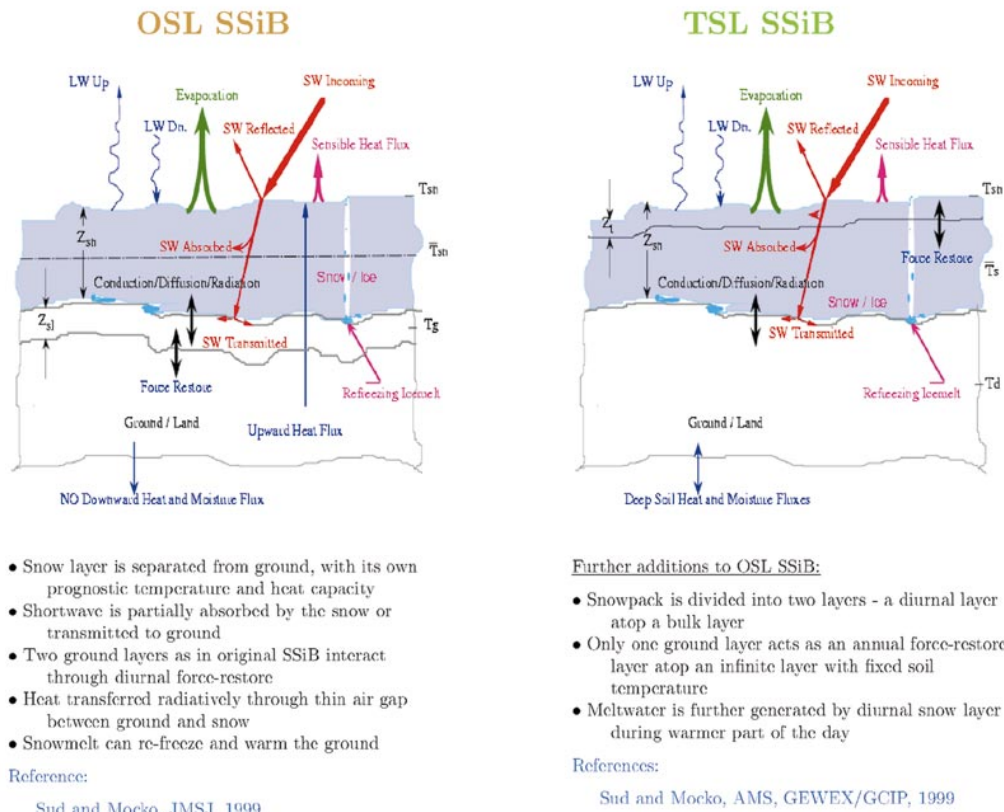


Figure 2. Schematics showing the major design features of two versions of the SSiB snow model. Left, OS�; right, TSL. The deep soil temperature T_{sd} in TSL is not shown as it is much below T_g .

The blended soil layer interacts with the bulk snowpack above it in virtually the same way as in OS�. Heat exchange between the soil and snow layers occurs by radiation through an assumed very thin air gap between them by radiation. It is natural to assume air gaps when considering the roughness and debris (including grasses) of the land surface together with natural aeration of snow. This air gap functions to introduce a timescale of 2 or 3 h in the exchange of heat between snow and soil. The incoming shortwave energy can be reflected, absorbed in the snow (in either of two snow layers), or transmitted through the snow and absorbed in the soil. The refreezing of snowmelt on top of the soil (if below the freezing temperature), which raises the soil heat content, as well as the snowmelt by ground heat flux are left unchanged from OS�. The additional feature of invoking the saturation pressure over ice (rather than over water) with a snowpack is also unaltered. Also as in OS�, the scheme holds the snow fluxes constant for melting conditions; this eliminates fictitious warming of snow and its influence on saturation vapor pressure in the implicit backward solution. For details on these processes, see Sud and Mocko (Sud and Mocko, 1999).

2.1.2 Age effect

Having experimented with a few documented algorithms, the age effect of the snow on snow density has been adopted following Verseghy (Verseghy, 1991). The snow density of the bulk snow layer is assumed to be constant with depth, and increases exponentially with time from the fresh snow value of $\rho_{s \text{ min}} = 100 \text{ kg m}^{-3}$ to $\rho_{s \text{ max}} = 300 \text{ kg m}^{-3}$, following

$$\rho_s(t + \Delta t) = [\rho_s(t) - \rho_{s \text{ max}}] \exp\left(-0.24 \frac{\Delta t}{\tau}\right) + \rho_{s \text{ max}}, \quad (1)$$

where ρ_s is the density in kilograms per cubic meter, $\tau = 86\,400 \text{ s}$, and Δt is the time step in seconds. The snow density can become more than $\rho_{s \text{ max}}$ as a result of refreezing of rain or meltwater, while fresh snowfall lowers the density via a weighted average of the old and new snow. The density of the diurnal snow layer is held at 120 kg m^{-3} so as to generate a constant-depth diurnal layer, which is approximately the ρ_s value from Eq. (1) after a 12-h half-day period.

The snow density affects two main parameters of TSL. The snow thermal conductivity κ_s is a strong function of the snow density. With some sensitivity experiments (not shown), it was found that making the snow conductivity a function of snow density has a large effect on the evolution of the snowpack. The form of the relation among the available literature had relatively little effect in test simulations, although Loth and Graf (Loth and Graf, 1998b) did show an effect in a different set of experiments. Regardless, the functional form due to Yen (Yen, 1981) is adopted in TSL:

$$\kappa_s = \kappa_i \left(\frac{\rho_s}{\rho_w}\right)^{1.88}, \quad (2)$$

where κ_s is the thermal conductivity of snow in watts per meter per kelvins, $\kappa_i = 2.22 \text{ W m}^{-1} \text{ K}^{-1}$ is the thermal conductivity of ice, and $\rho_w = 1000 \text{ kg m}^{-3}$ is the density of water.

2.1.3 Fractional snow cover

The fractional snow cover on the ground in TSL is also defined as a function of the snow density, as well as of the snow depth. The water equivalent snow depth multiplied by the density of water and divided by the density of snow gives the depth of the snow. If the water equivalent snow depth is below 10^{-5} m , the snow fraction is arbitrarily set to zero. Above 10^{-5} m depth, the snow cover fraction is developed with the following functional form:

$$\epsilon = \exp \left[-2 \left(\frac{\alpha Z_{st} \rho_w}{\rho_s} - \beta \right) \right], \quad (3)$$

$$\gamma = - \frac{1 - \exp(2\beta)}{1 + \exp(2\beta)}, \quad (4)$$

$$F_s = \frac{\left(\frac{1 - \epsilon}{1 + \epsilon} \right) + \gamma}{1 + \gamma}, \quad (5)$$

where F_s is the fractional snow cover (dimensionless, from 0 to 1), Z_{st} is the total water equivalent snow depth in meters, α is 35 m^{-1} , and the β coefficient is 2. The relation of fractional snow on the canopy is unmodified from original SSiB.

Figure 3 shows a few representative curves for fractional snow cover as a function of water equivalent snow depth based on snow density. This function (along with the associated parameters) in TSL is designed to increase the fraction slowly at first, then increase rapidly before asymptoting to 1.0. The function produces fractional snow cover values generally comparable to values from a number of recent models in the available literature. The fractional snow cover then affects the four components of albedo (direct/diffuse, visible/near-IR) and the radiation absorption coefficients within SSiB. These radiation parameters are also affected by melting snow. If either the diurnal or bulk snow layer temperature is greater than 272.16 K, the snow is considered to be in a melting phase or recently melted, which reduces the snow albedos and coefficients to 60% of their values. Similar assumptions were already used in SSiB. For details on how these parameters are calculated, see Xue et al. (Xue et al., 1991) and Sellers et al. (Sellers et al., 1986).

2.1.4 Deep soil temperature

Another significant change to the calculation of soil temperatures is in the bottom heat flux due to heat exchange with the infinite ground beneath, which happens regardless of the snow cover. A calculation for heat exchange between the deep soil temperature T_d and a constant “very deep” soil temperature T_{dd} is added. A force–restore on an annual timescale determines the heat exchange and time rate of change (in K s^{-1}) of T_d :

$$\frac{\partial T_d}{\partial t} = \frac{2\pi}{365\tau} (T_{dd} - T_d), \quad (6)$$

where T_{dd} for each grid box was obtained by doing a multiyear average of T_d (all temperatures in K). As will be shown later, adding Eq. (6) to the model has the beneficial effect of improving the amplitude of the annual cycle of deep temperature by cooling the deep (and by extension, the diurnal soil temperature T_g) layer during the summer, and by warming the soil from below during the winter. If the multiyear average T_{dd} is warmer than freezing in a particular snow-covered area, adding this equation to the system will warm the soil under the snowpack during

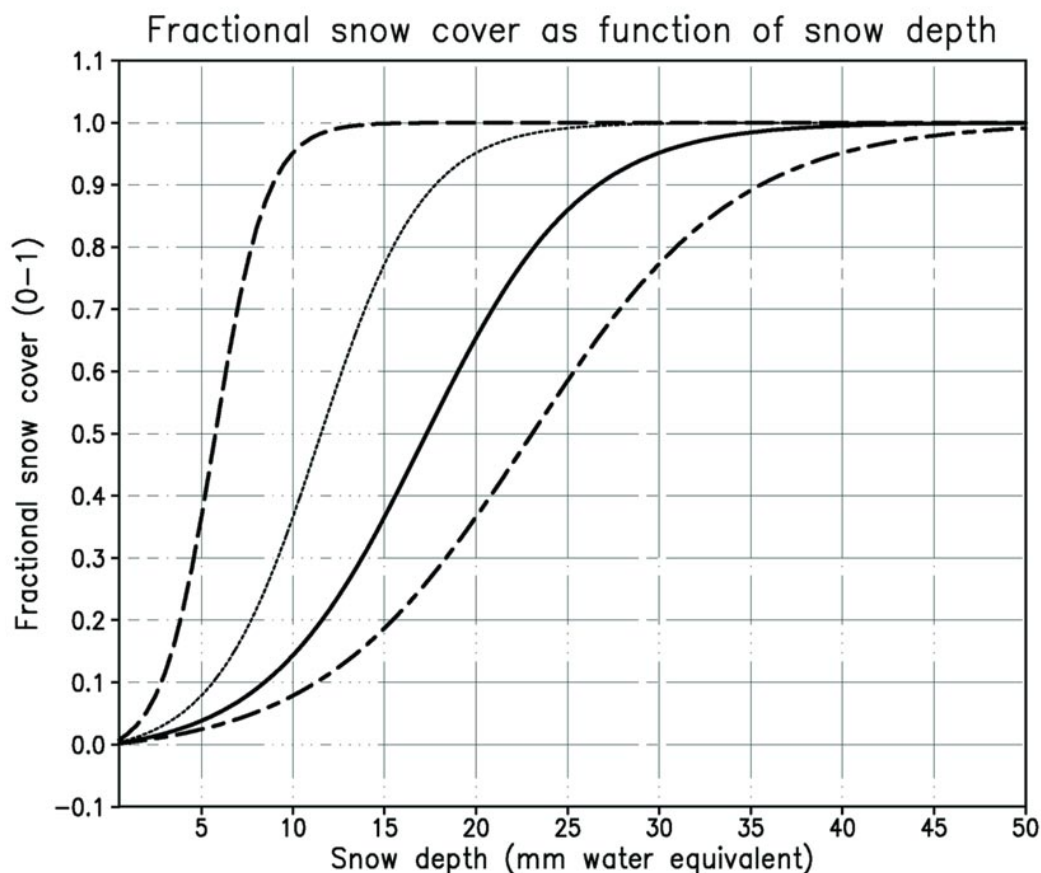


Figure 3. Fractional snow cover as a function of water equivalent snow depth for several representative snow densities: long dash, 100 kg m^{-3} ; short dash, 200 kg m^{-3} ; solid, 300 kg m^{-3} ; and intermittent dash, 400 kg m^{-3} .

winter. The warmer soil temperature can produce or cause earlier melting and meltwater infiltration. This modification is physically based and the new correction generally improves the simulation.

2.2 Changes to the hydrology model

2.2.1 Orography-based runoff

SSiB did not parameterize a dependence of overland flow for high orography. The need for this is evident, although it is difficult to design such a parameterization. In the original SSiB, the only two ways that surface flow could occur were 1) soil wetness fractions exceeding 1.0 or 2) due to infiltration of precipitation (especially convective vs large scale) described in Sato et al. (Sato et al., 1989) and Sellers et al. (Sellers et al., 1996). The function of the distribution equation is

$$PI(x) = (P_c a_c + P_p a_p) \exp^{-bx} + (P_c c_c + P_p c_p), \quad (7)$$

where P_c and P_p are the convective and large-scale precipitation rates (respectively) in millimeters during the time step and $PI(x)$ can be interpreted as an amount distribution that is used to calculate throughfall and infiltration rates. The dimensionless coefficients (a , b , c) for convective and large-scale precipitation are recast to better match observed runoff values with simulated in nearly 30 basins around the globe for GSWP-style simulations for 1987–88. The original and new TSL values are shown in Table 1.

Table 1. Current and original values for the dimensionless coefficients for the amount distribution of precipitation in SSiB.

Version of SSiB	a_c	b	c_c	a_p	c_p
TSL	5.0	5.0	6.737946e-3	0.0001	0.9999
Original	20.0	20.0	0.206e-8	0.0001	0.9999

The runoff from melting snow cover, which had been excessively high in the original SSiB, was systematically reduced in OSL. Additionally, the values of runoff were low compared to observations from many river basins on the annual timescale. Therefore, a hillslope orography function is constructed that runs off a fraction of the available water (AW—primarily, rainfall and meltwater) before it has a chance to enter the soil. The simplest functional form in which the runoff fraction is a function of the soil slope did not show much promise. However, with the availability of the GTOPO30 digital elevation model (DEM) orography heights at a horizontal grid spacing of 30 arc sec, the runoff fraction is reformulated as a function of the standard deviation of the orography height σ_h (in m) in each 1° by 1° grid box. The σ_h was calculated from the height at each grid box in the GTOPO30 DEM to the mean of the DEM heights in the 1° box. After a global map of σ_h was constructed, the annual runoff deficit (observed runoff minus modeled runoff from OSL) was calculated for 29 river basins around the globe with observed runoff data for 1987–88 and a sufficient number of rain gauges in the basin (after Oki et al., 1999). Next, the water available for runoff (AW—precipitation plus meltwater minus snowfall) was calculated for the same basins on an annual basis. These values are shown in a scatterplot, with the σ_h scaled by $\sigma_{h \max} = 1840$ m, and the runoff deficit scaled by AW. To reduce the potential dominance of a few grid boxes in the basin, the σ_h was weighted by the AW at each grid box, then averaged over the basin, then divided by the basin-averaged AW. A fit is drawn to this scattered data and is shown in Figure 4. The final form of the function for orography-aided surface runoff is

$$AR = \min \left[\left(2.07 \frac{\sigma_h}{\sigma_{h \max}} \right), 0.5 \right] AW, \quad (8)$$

where AW represents the available surface water in meters at any time during the model time step and AR is the additional runoff generated in meters. The precipitation contribution to AW is calculated after the runoff produced via Eq. (7), and the meltwater contribution to AW does not include refreeze. The development of Eq. (8) was done assuming a 1° grid; however, it may be applicable

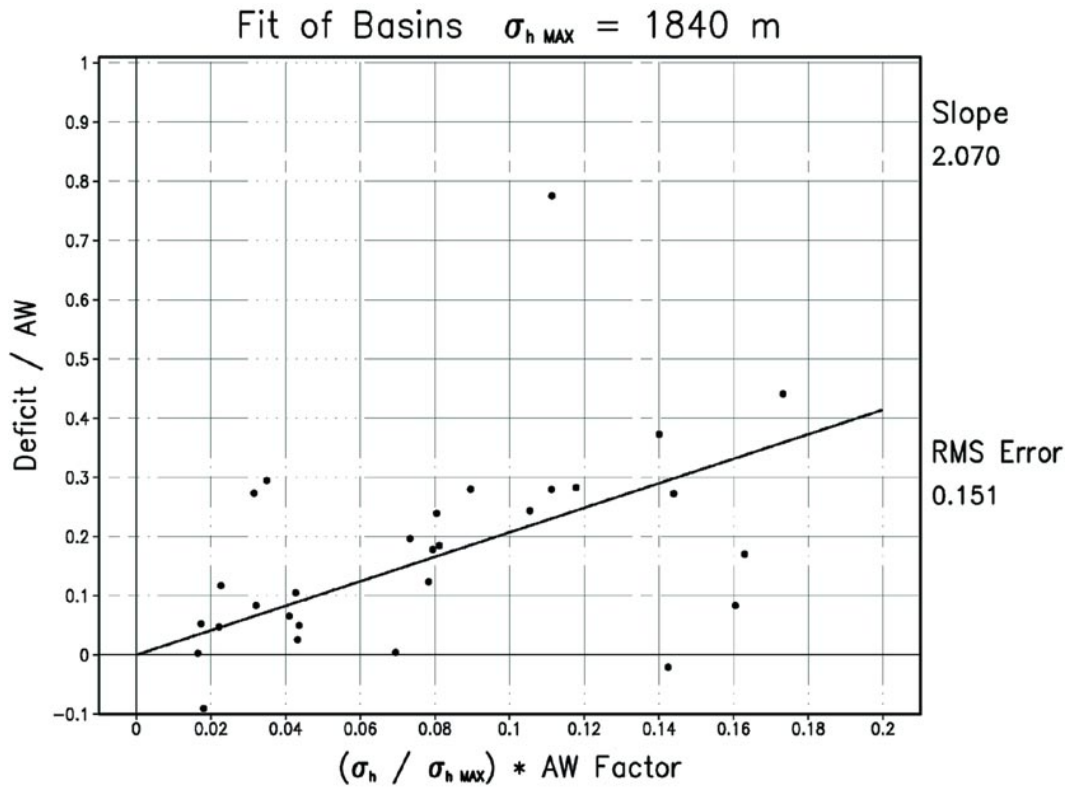


Figure 4. Scatterplot and least squares approximation for annual runoff deficit values by standard deviation of orography for 29 basins around the globe for 1987–88 data.

to other grid scales as the basins used to fit this curve have a wide range of sizes and locations.

2.2.2 Linear reservoir drainage

Some improvements are also made to the linear reservoir drainage of SSiB. Liston et al. (Liston et al., 1994) introduced a calculation for discharge from the bottom layer that accounts for the spatial variability of the grid box. This equation has been recast as

$$BF = \left(\frac{\Delta t}{365\tau} \right) (W_3 - W_{\text{wilt}}) P Z_3, \quad (9)$$

where BF is the subsurface runoff (or baseflow) in meters from soil moisture layer 3 during the time step, and Z_3 is the depth of soil moisture layer 3 in meters. Here, W_3 is the soil wetness of layer 3, W_{wilt} is the wilting point wetness (see Mocko and Sud, 1998), and P is the soil porosity (all dimensionless).

2.2.3 Gravitational drainage

The gravitational drainage in SSiB is also modified accordingly. The equation essentially is unchanged, other than the drainage had been the minimum of Sellers et al. [Sellers et al., 1986, Eq. (62)] and $W_3 P Z_3 / \Delta t$, and now the minimum has been replaced by $(W_3 - W_{\text{grav}}) P Z_3 / \Delta t$, where

$$W_{\text{grav}} = \left(\frac{\psi_s - 0.5Z_3}{\psi_s} \right)^{-(1/B)} \quad (10)$$

is the dimensionless wetness at which Z_3 is half-saturated, ψ_s is the soil moisture potential at saturation in meters, and B is the dimensionless Clapp and Hornberger (Clapp and Hornberger, 1978) parameter. If W_3 is below W_{grav} , this half of the minimum is zero, and gravitational drainage does not occur.

2.2.4 Water table interaction

An important change to SSiB's hydrology is the addition of a water table interaction below soil moisture layer 3. If W_3 happens to drop below W_{wilt} , a factor is put into place such that half of this loss during the time step is replaced by the water table. To make this calculation, the water table height is assumed to be at the level of the bottom of soil layer 3, and the baseflow and gravitational drainage described above will move water back from W_3 to the water table during wet periods. An elementary parameterization of the effects of a rising and falling water table is thus introduced to keep the very deep soil from going too dry (wet) in a prolonged drought (rainy) period.

2.3 Changes to the calculation of SSiB fluxes

2.3.1 Bare soil evaporation

Several changes are made to the way SSiB calculates surfaces fluxes and how the soil responds to these fluxes. The bare soil evaporation and transpiration rates calculated by SSiB have remained the same; however, the depth at which the water is removed from the soil has been changed. For bare soil evaporation, the water can now be removed from any of the three layers—on the assumption that scattered capillaries of various shapes and forms (nonwater areas) in the soil allow vapor from the lower layers to pass through to the surface. The extraction from each of the three layers is weighted by the fractional weight for each layer, divided by the sum of the three weights. The dimensionless weights WTB_i for each of the three layers are

$$WTB_1 = \exp \left[\left(\frac{\psi_s g}{R_v T_g} \right) W_1^{-B} \right], \quad (11)$$

$$WTB_2 = (1.0 - WTB_1) \left(\frac{2Z_1}{2Z_1 + Z_2} \right) \exp \left[\left(\frac{\psi_s g}{R_v T_g} \right) W_2^{-B} \right], \quad (12)$$

$$WTB_3 = (1.0 - WTB_1 - WTB_2) \left(\frac{2Z_1}{2Z_1 + 2Z_2 + Z_3} \right) \exp \left[\left(\frac{\psi_s g}{R_v T_g} \right) W_3^{-B} \right], \quad (13)$$

where $g = 9.81 \text{ m s}^{-2}$ is the acceleration due to gravity at the Earth's surface; $R_v = 461.5 \text{ J K}^{-1} \text{ kg}^{-1}$ is the water vapor gas constant; Z_i and W_i is the depth (in m) over soil moisture layer i and soil wetness (dimensionless) of layer i , respectively; and T_g is the temperature of the top soil temperature layer (in K). Although some soil water extraction can now be realized from layers 2 and 3, the vast majority of the weighting still takes bare soil evaporation loss from soil moisture layer 1.

2.3.2 Extraction by transpiration

The extraction of water from the soil that is used in transpiration is similarly modified with a weighted fraction taken for each of the layers containing vegetation roots. Additionally, the dimensionless weight for each layer WTT_i is set to zero if the soil moisture potential of that layer ψ_i (in m) is less than a minimum of soil moisture potential ψ_{low} (in m). These weights are calculated as

$$\psi_i = \psi_s W_i^{-B}, \quad (14)$$

$$\psi_{\text{low}} = \psi_s W_{\text{wilt}}^{-B}, \quad (15)$$

$$\text{WTT}_i = (\psi_i - \psi_{\text{low}}) Z_{i \text{ root}}, \quad (16)$$

where $Z_{i \text{ root}}$ is the depth (in m) of layer i that contains roots. The parameter ψ_{low} also is used as a minimum when calculating the stomatal resistance parameter shown in Xue et al. [Xue et al., 1991, Eq. (9)].

2.3.3 Buoyancy velocity scale

The bulk aerodynamic formula for the sensible heat flux in SSiB is modified, after Mahrt and Sun [Mahrt and Sun, 1995, Eqs. (11) and (12)]. The revised formula includes a “buoyancy velocity scale” in meters per second defined by

$$w_B = \left(\frac{g}{\theta_v} z_i \Delta \theta_B \right)^{1/2}, \quad (17)$$

where z_i is the boundary layer depth in meters, and $\Delta \theta_B$ in kelvins is the difference between the virtual potential temperature at the surface θ_v in kelvins and the virtual potential temperature of the mixed layer. The new buoyancy velocity scale is added to SSiB's wind speed M in meters per second at reference height as

$$M = M + (2b_H w_B C_{\text{TN}}^{-1} C_{\text{UN}}^{-1}), \quad (18)$$

where $b_H = 0.00025$, and C_{TN} and C_{UN} are SSiB's neutral heat and neutral momentum transfer coefficients, respectively (all dimensionless). This scale is added for unstable cases only. It is introduced before the calculation of the aerodynamic resistance between the canopy air space and the reference height. The minimum reference height wind speed is also changed from 2.0 to 0.1 m s^{-1} . This is a physically based upgrade, and it has the benefit of increasing sensible heat flux and leading to some, though not full, correction of anomalously warm skin temperatures over hot dry desert regions by SSiB.

Two other changes are made to the SSiB flux calculations. The first is that

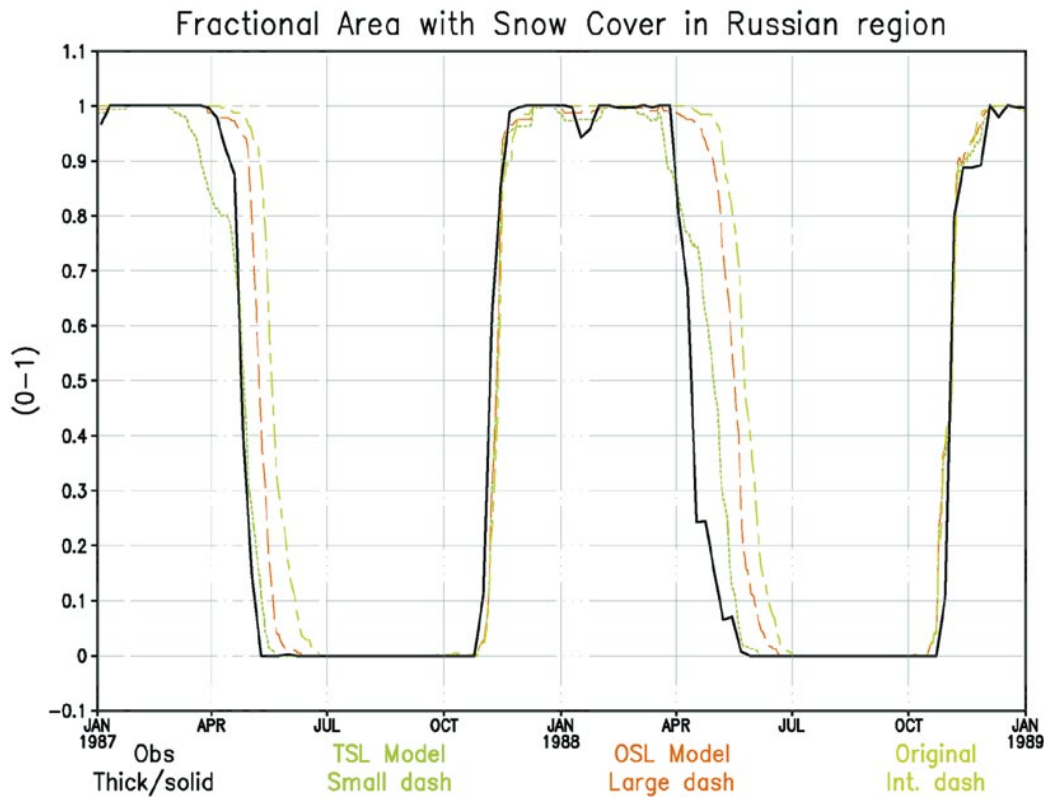


Figure 5. Line plot showing area-averaged snow cover fraction (0-1) in the Russian Wheat Belt region for 1987-88, same as in Figure 1 but with the addition of a short-dashed line, which is from TSL.

SSiB biome type 11 (desert) in OSL did not explicitly calculate the stomatal resistance, whereas TSL does. The second is that the maximum stomatal resistance for the canopy layer for any given biome type (and the constant value for all ground story layers) is changed from 1.0^5 to 1.0^{10} in seconds per meter. These changes allow SSiB to cover a wider range of resistances to calculate the stomatal resistance on its own (especially for desert) reducing the influence of an arbitrary cutoff although either maximum condition is only very infrequently met.

3. Results with GSWP global data

The upgraded version of the snow-physics scheme with SSiB was integrated globally for 1987-88 using the 1° by 1° ISLSCP Initiative I data after a 10-yr soil moisture spinup procedure. The procedure followed is the same as for previous versions of SSiB and is described in Dirmeyer et al. (Dirmeyer et al., 1999). The ISLSCP Initiative I data is a 6-hourly set of global atmospheric forcing fields. Near-surface values for pressure, temperature, humidity, and wind speed are from

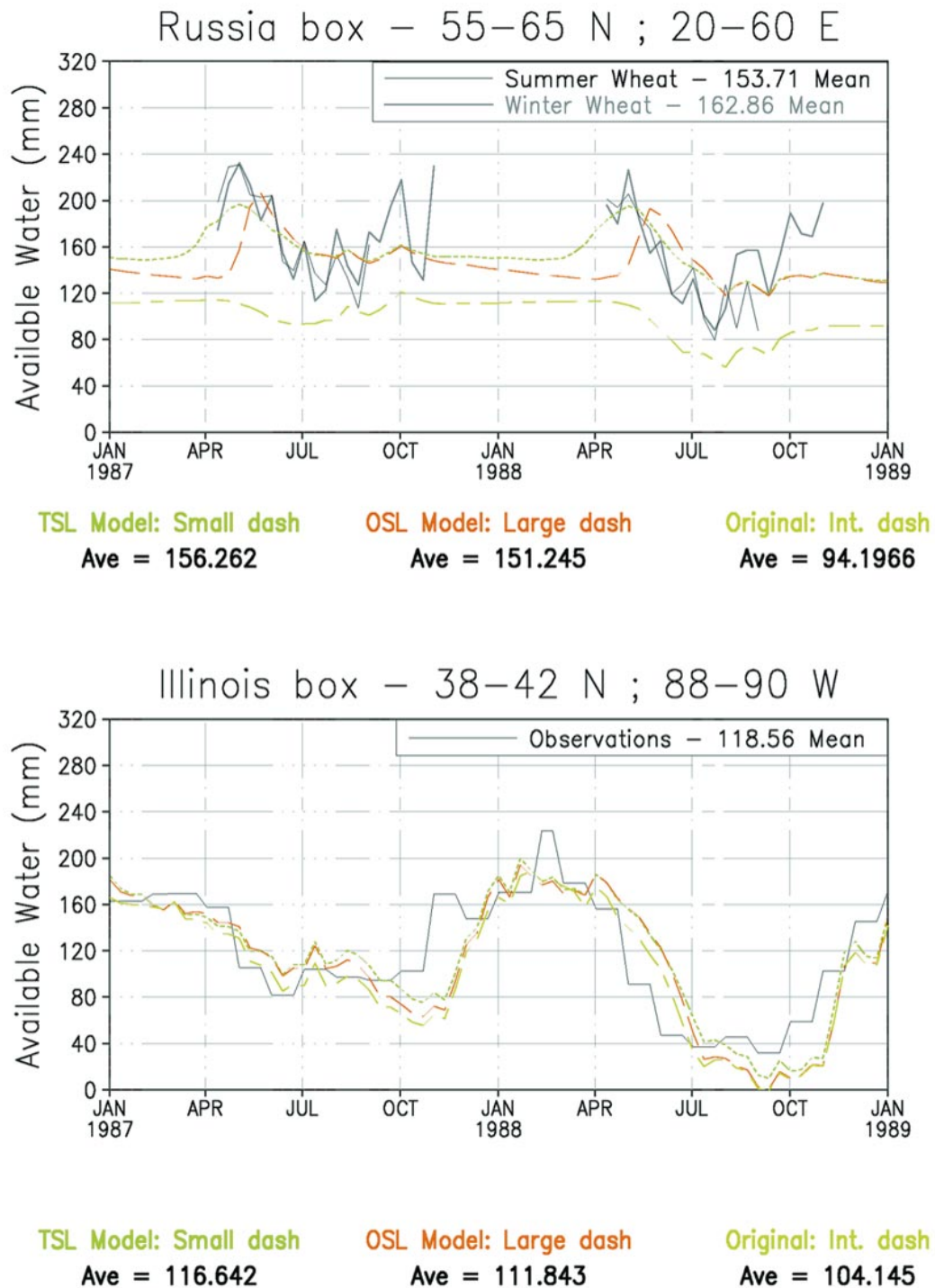
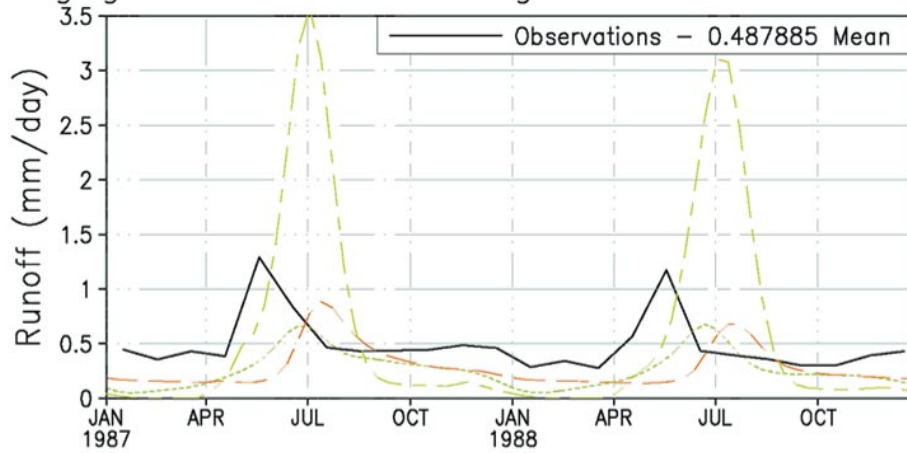


Figure 6. Time series of available water in millimeters for (top) the Russia Wheat Belt region and (bottom) Illinois for TSL, OSL, and the original SSiB and observations (along with annual averages).

Volgograd Plant RS in Volga 6977100 48.5N 44.5E

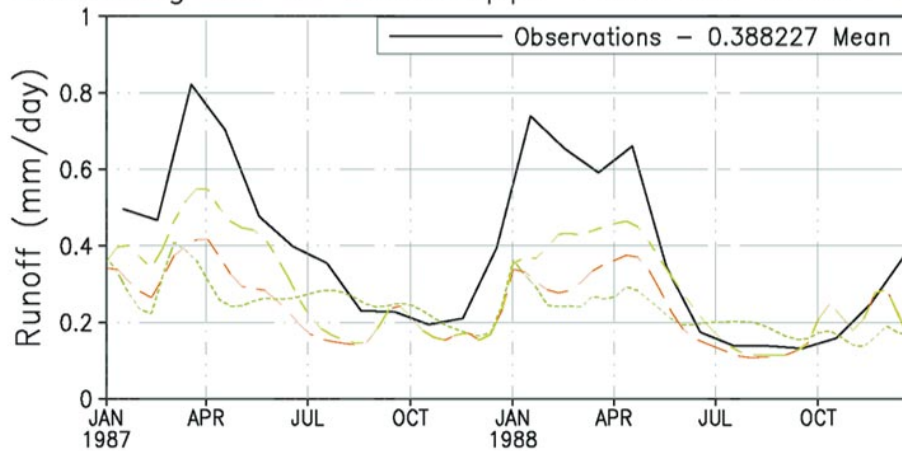


TSL Model: Small dash
Ave = 0.262054

OSL Model: Large dash
Ave = 0.283342

Original: Int. dash
Ave = 0.587457

Vicksburg MS in Mississippi 4127800 32.5N 91.5W



TSL Model: Small dash
Ave = 0.238453

OSL Model: Large dash
Ave = 0.238854

Original: Int. dash
Ave = 0.289153

Figure 7. Time series of TRIP-routed streamflow (mm day^{-1}) for (top) the Volga River basin in the Russia Wheat Belt region and (bottom) the Mississippi River basin for TSL, OSL, and the original SSiB and observations from gauges (along with annual averages).

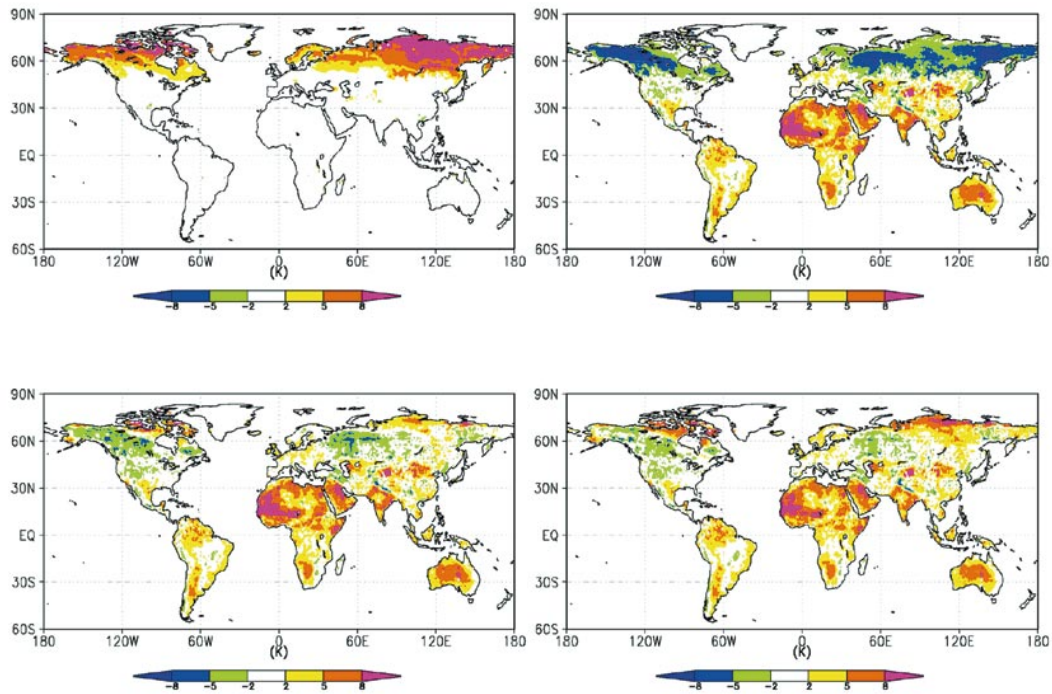


Figure 8. Differences for May 1987 in global monthly averaged skin temperatures (K) between simulated and observations taken from satellite: (upper left) TSL minus original SSiB, (upper right) the original SSiB minus the satellite observations, (lower left) OSL minus the satellite observations, and (lower right) TSL minus the satellite observations.

European Centre for Medium-Range Weather Forecasts (ECMWF) analysis; precipitation values are from a combination of monthly Global Precipitation Climatology Project (GPCP) data and National Centers for Environmental Prediction (NCEP) reanalysis data; surface radiation values are from a combination of monthly International Satellite Cloud Climatology Project (ISCCP) data and ECMWF analysis. Values were linearly interpolated to an hourly time step, with the exception of the downward shortwave radiation, which took into account the solar zenith angle to reproduce a realistic diurnal cycle. Downward longwave radiation values, which are difficult to obtain accurately on this scale, have been shown to have a large influence on the simulation of snowmelt (Slater et al., 1998). Morrill et al. (Morrill et al., 1999) showed a possible error with the ISLSCP Initiative I longwave data, which led to the longwave data being shifted 6 h earlier to produce realistic diurnal cycles.

The Russian Wheat Belt region (55° – 65° N, 20° – 60° E) is again studied because of the availability of observations of soil moisture and runoff in this area. Northern Hemisphere observations of snow cover from satellite data are also available through the ISLSCP Initiative I dataset. The weekly data are retrieved

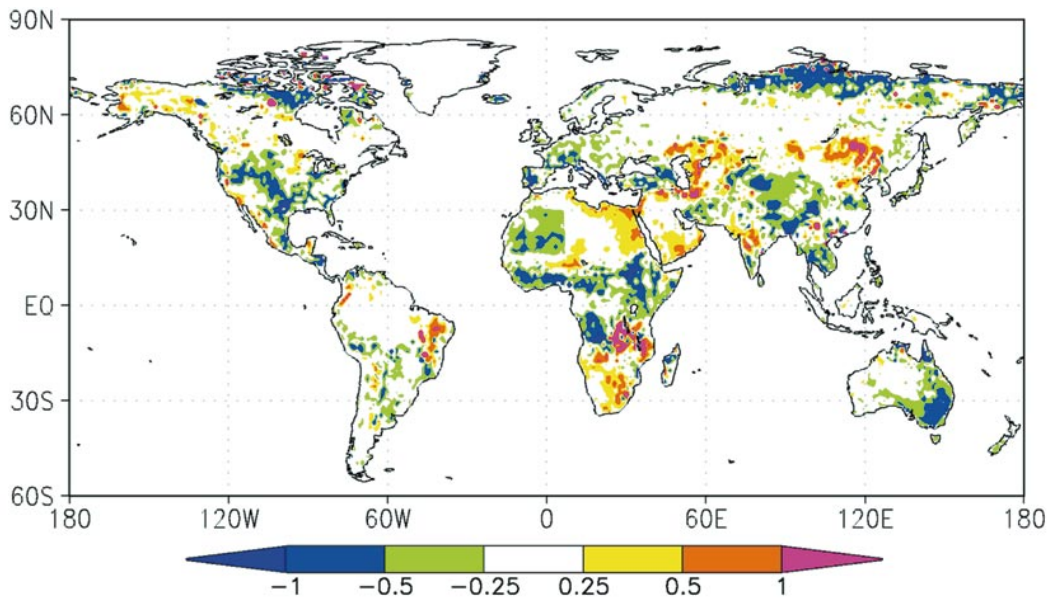


Figure 9. Difference between using and not using the buoyancy velocity scale in the TSL version of the model for May 1987 in the simulated skin temperatures (K).

from National Oceanic and Atmosphere Administration (NOAA) satellites and each individual satellite cell (on an 89 by 89 cell Northern Hemisphere grid) is considered either snow free or snow covered. By taking an area-averaged time series of observed snow cover of this region and comparing it to similar curves from the simulated model data, as shown in Figure 5, one can see that TSL does a better job of simulating snowmelt timing. In addition, TSL also captures some of the midwinter snowmelt in January 1988 that previous versions did not. This benefit results from the diurnal layer of the snowpack, which is able to melt more realistically during warm winter episodes.

Over this time period, there are two useful soil moisture validation datasets. One, a portion of which includes the Russia Wheat Belt region, is described by Vinnikov and Yesserkepova (Vinnikov and Yesserkepova, 1991); the other, in the state of Illinois in the central United States, is described by Hollinger and Isard (Hollinger and Isard, 1994). The time resolution of these data is generally a week to 10 days; however, the Russian data are not available in winter due to soil freezing. These data are compared against the simulated soil moisture data in terms of available water in the top meter of the soil, which is simply the total water in the top meter minus the soil's wilting point value. The simulated versus observed values are shown in Figure 6. In the top part of the figure for the Russian region, the effect of the soil moisture spinup is clearly seen as TSL has wetter soil than the original. TSL also better reproduces the spring rise in soil moisture due to meltwater infiltration, followed by drying in the summer from evapotrans-

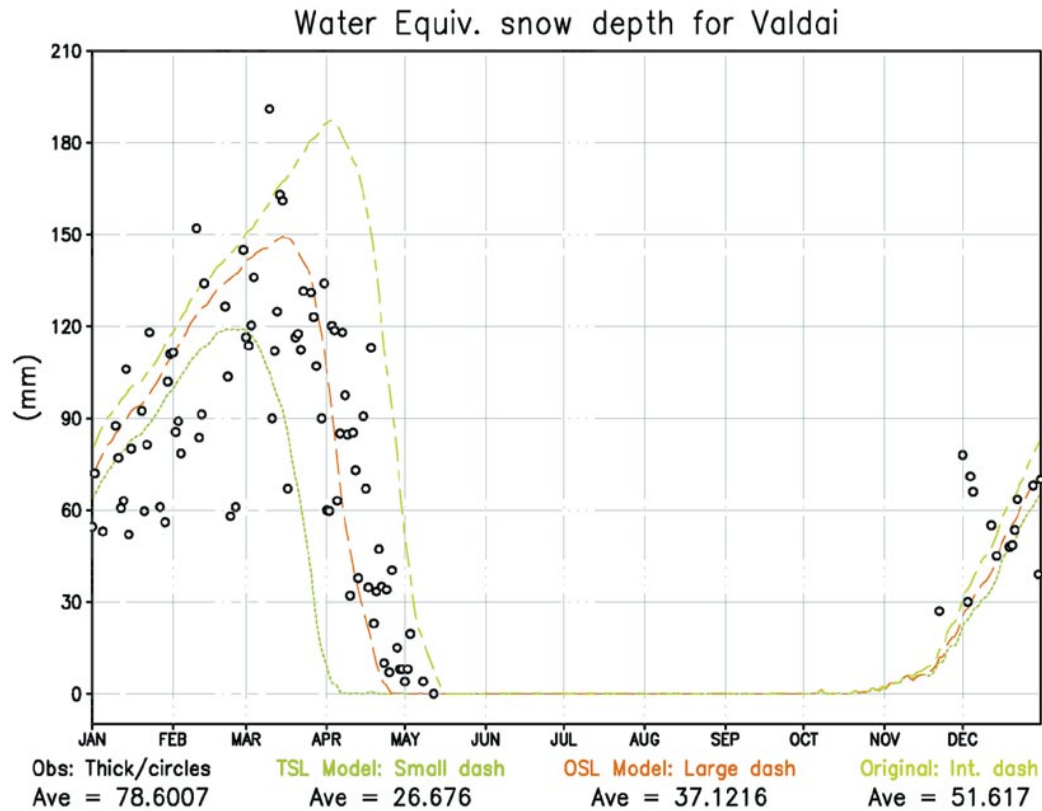


Figure 10. Annual averaged water equivalent snow depth in millimeters for the 18-yr Valdai, Russia, simulation. TSL is shown with a small dash, OSL is shown with a large dash, and the original SSiB is shown with a variable dash. The observations are shown as circles plotted at the time of year of the measurement.

piration. OSL also produces a spring rise, but it is delayed after the peak in the observations. In the bottom part of the figure for Illinois, where there is less meltwater generated and the change in the snow physics has relatively little effect, the simulated soil moisture from TSL, OSL, and original SSiB compare well with observations. All versions of SSiB do capture the wet 1987 and dry 1988 in Illinois. However, TSL is wetter than the other two versions of SSiB on the annual timescale in better agreement with the observations. In addition, TSL has the wettest late summer and fall, showing the beneficial effects of the water table interaction.

The simulated against observed basin-scale runoff is also a worthy tool for validating a land surface scheme. However, to be truly useful, the simulated runoff should be routed through a river routing scheme. The simulated runoff by all three versions of the model were separately routed using the Total Runoff Integrating Pathways (TRIP) river routing network of Oki and Sud (Oki and Sud,

1998) and used in Oki et al. (Oki et al., 1999). The TRIP-routed runoff for two river basins compared to observations from streamflow is shown in Figure 7. These basins were chosen because they had available river gauge observations that were close to the soil moisture regions defined in Figure 6. The top part of the figure shows the simulated and observed flow in the Volga River, which is in the Russia Wheat Belt region. One easily notes the spuriously high and late runoff in the original SSiB. TSL has an earlier spring peak in the flow (from meltwater) than OSL. The bottom of the figure is for the Mississippi River basin in the central United States. The annual flow is generally similar to OSL, except the June to October flow is higher in TSL as a result of the modifications to baseflow.

Another useful land surface scheme validation variable is skin temperature. This value can be retrieved from a satellite, where it is measured over the satellite pixel size, or simulated by a model, where it is the spatial average of the vegetation and soil skin temperatures weighted by the fractional vegetation cover. Satellite-derived skin temperature values are prone to errors, particularly in regions with high amounts of dust aerosols. In addition, the solar radiation reaching the surface used as input to the land surface model can be in error because of the effects of atmospheric aerosols on solar radiation (e.g., Alpert et al., 1998). A useful satellite dataset for this time period is that of the TIROS (Television and Infrared Observation Satellite) Operational Vertical Sounder (TOVS) Pathfinder Path A in Susskind et al. (Susskind et al., 1997). The skin temperature differences between the model-simulated values and the satellite retrievals are shown in Figure 8. The upper-right panel shows a cold bias in the Northern Hemisphere in the original SSiB. This is from snow cover being simulated in the model but not observations. OSL in the lower-left panel removes most of this error, but the closest values to the observations are found in TSL, as shown in the lower-right panel. Especially in the Russia Wheat Belt region and northwestern Canada, TSL is more realistic than OSL in the simulated skin temperature comparison.

Additionally, adding the Mahrt and Sun (Mahrt and Sun, 1995) buoyancy velocity scale to the surface wind speed has the effect of partially mitigating a warm bias in surface temperatures between OSL and TSL in hot and dust-prone regions. A closer look at this result is shown in Figure 9, where in regions of the Sahara, Australia, and the western United States the skin temperatures have cooled by about 1 K. Other areas of cooling are found in India and the Middle East in northern winter (not shown). This calculation uses arbitrary constants and can be improved to produce better results.

4. Results with the Valdai region data

All three versions of the SSiB were integrated using an 18-yr single-site dataset from Valdai, Russia. These data are described in Vinnikov et al. (Vinnikov et al., 1996) and Schlosser et al. (Schlosser et al., 1997); it is a midlatitude grassland field and was used for PILPS Phase 2(d) (Schlosser et al., 2000). The years of the simulation are 1966–83 and the area is noted for its deep snowpack in winter that is followed by a strong spring melt. The data used are from the Usadievskiy catchment at Valdai where the long-term measurements were taken. Before the

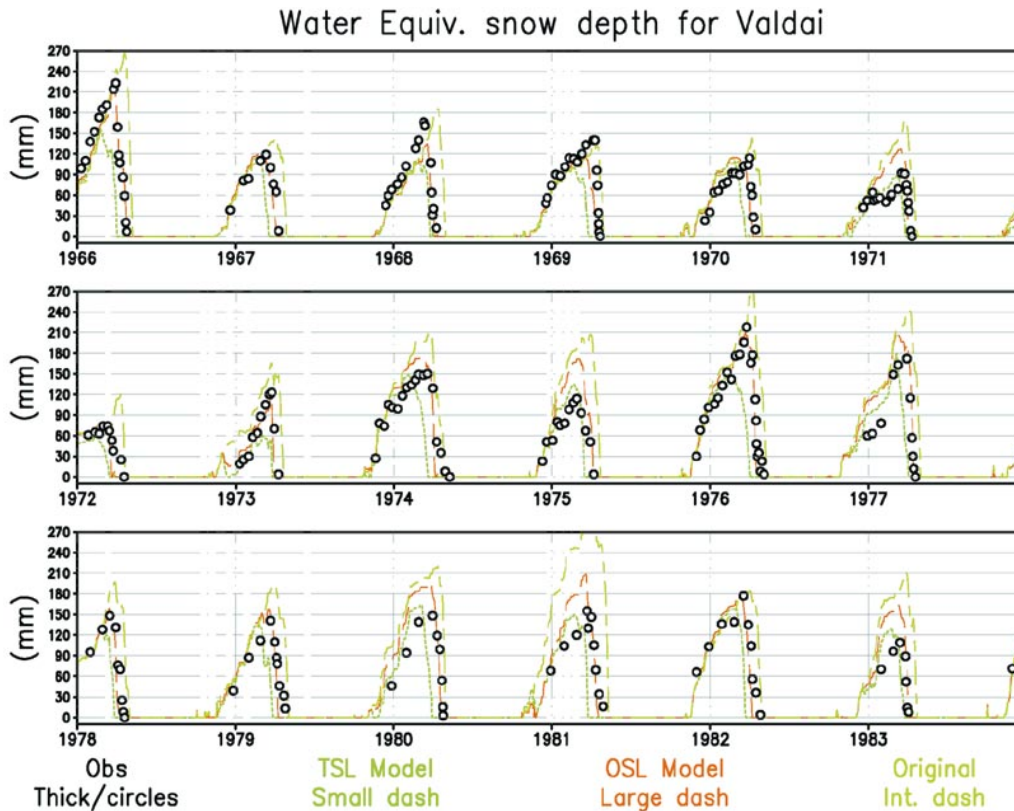


Figure 11. Same as in Figure 10, except now showing an 18-yr time series of the water equivalent snow depth (mm).

18-yr simulation began, each version's initial soil moisture was separately spun up using the 1966 forcing data until the soil moisture reached a quasi equilibrium.

The annual cycle of snow accumulation and snowmelt is shown in Figure 10. The observations, which are recorded monthly (and after snow events and frequently during snowmelt), are shown in circles. As discussed in the GSWP simulations, the original SSiB simulates much delayed snowmelt, while TSL has the earliest snowmelt. There is some indication that TSL may be melting snow too early, although it is somewhat difficult to isolate a systematic bias. A better picture of this early melt is shown in Figure 11, which is a time series over the entire 18 yr. For many spring melt periods, TSL is too early. However, TSL does well for some years in simulating the maximum snow depth, certainly no worse than OSL. TSL is also shown to have periods of midwinter melt, doing a particularly nice job of reproducing the winter 1971 snow depth. The early melt in some Valdai winters may be sensitive to arbitrarily chosen values for T_{ad} , ρ_s for the diurnal layer, or κ , given before or in the appendix. Additionally, the terrestrial albedo simulated by all three versions is around 0.61, where the observed maximum snow albedo at this site is around 0.75 (Schlosser et al., 2000). If the

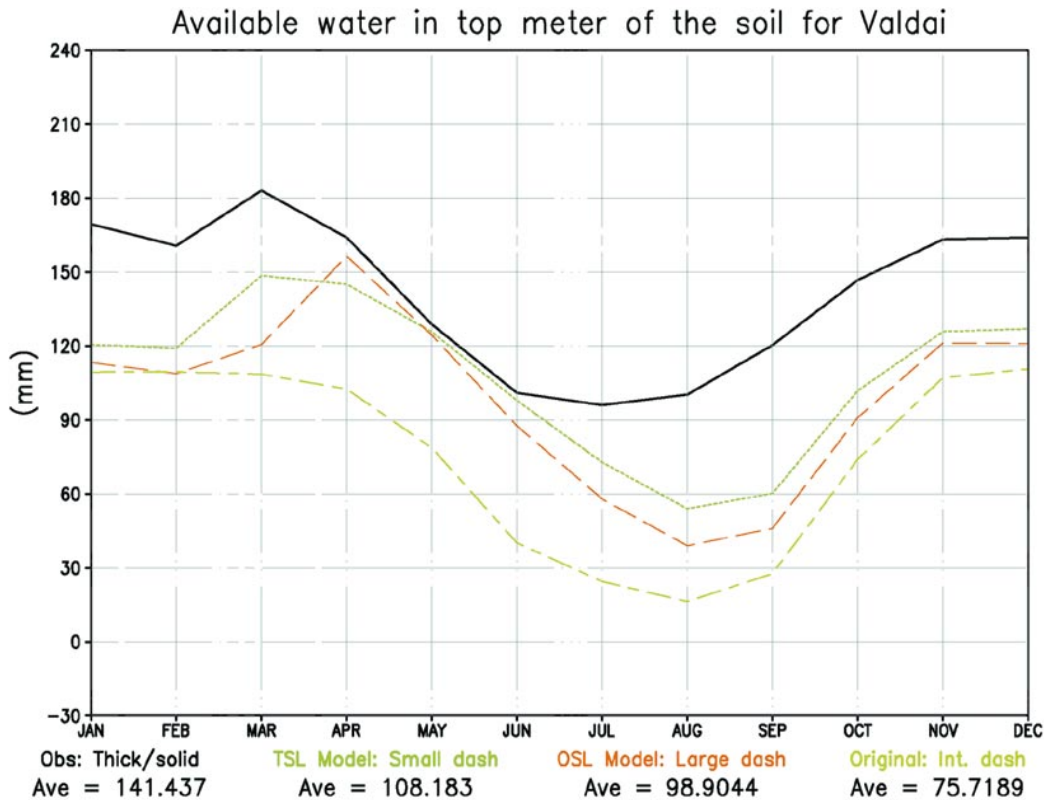


Figure 12. Same as in Figure 10, except for the annual averaged soil moisture (mm) in the top meter of the soil. The observed values are shown with a thick solid line.

simulated albedo is too low, it can produce excess solar energy absorption in the snow and soil and may be the root cause of early melt. Furthermore, the snow albedo depends upon the meltwater trapped on the surface. However, other factors such as the fractional snow cover, which determines the amount of solar radiation absorbed by the surface, may also be incorrect.

TSL does a better job of simulating the annual cycle of soil moisture as shown in Figure 12. The spring rise and March peak in soil moisture due to meltwater infiltration is captured quite well. The peak from OSL is too late, while original SSiB is too dry all year with no spring soil moisture peak. TSL (as well as OSL and the original SSiB) is found to be too dry in late summer, in part due to too high evapotranspiration (shown later). Still, the annual average simulated soil moisture is highest with TSL. The 18-yr time series of soil moisture is seen in Figure 13. Of particular interest is the simulated soil moisture profiles for the years 1976–77. The soil moisture in TSL remains closer to the observations for these 2 yr than original SSiB. Evidently, the spring 1976 rise in soil moisture helps to maintain better agreement with observations for the next 2 yr. Soil mois-

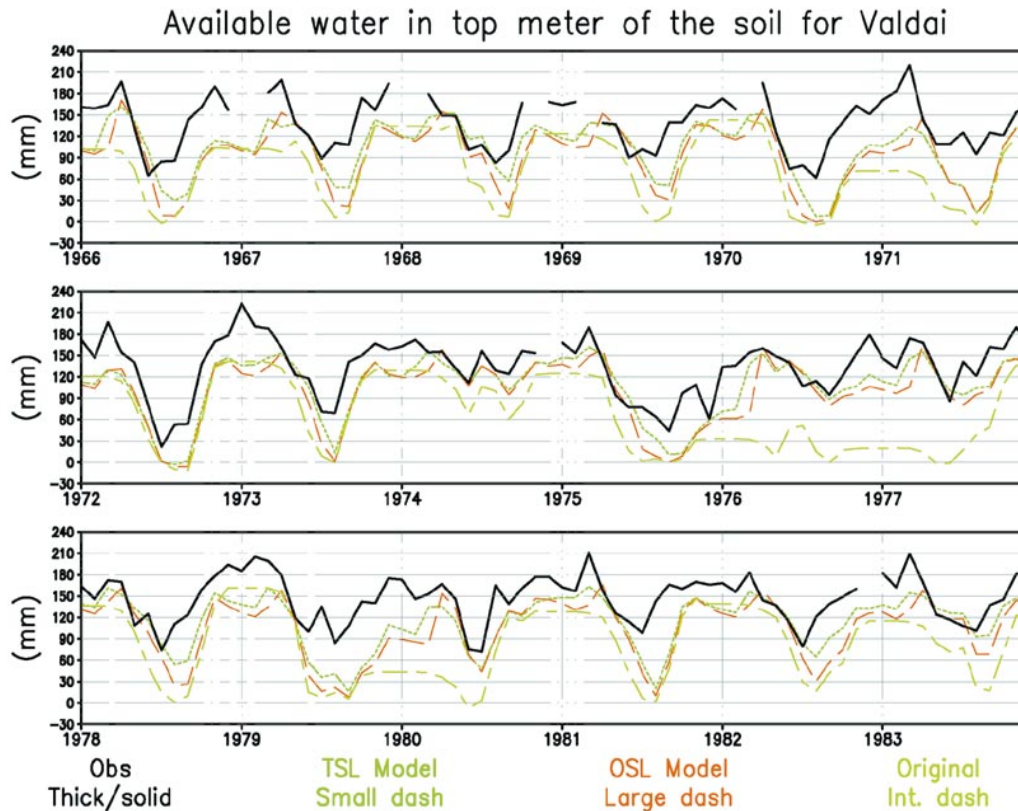


Figure 13. Same as in Figure 12, except now showing an 18-yr time series of the soil moisture (mm) in the top meter of the soil. Breaks represent missing data periods.

ture is difficult to measure accurately; see Vinnikov and Yeserkepova (Vinnikov and Yeserkepova, 1991) for a discussion of error estimates and variability of soil moisture in this area.

The annual averaged runoff at the Valdai location is shown in Figure 14. These catchment discharges are not routed through TRIP, as the Valdai region is sufficiently small. As before, the runoff from the original SSiB is too high and too late in the season. OSL has a very low spring soil moisture peak. In TSL, there is a strong initial peak in the runoff, but this drops off suddenly. The late summer and fall runoff is reproduced well, but the annual average of both TSL and OSL are too low for this region. This may be caused by too high simulated evapotranspiration.

The annual cycle of evapotranspiration is shown in Figure 15. TSL simulates well the early spring evapotranspiration as a result of the earlier snowmelt and meltwater infiltration. However, the simulated summer evapotranspiration in TSL and OSL are too high leading to too dry simulated soil moisture in the late summer and too little simulated annual average runoff (both shown earlier).

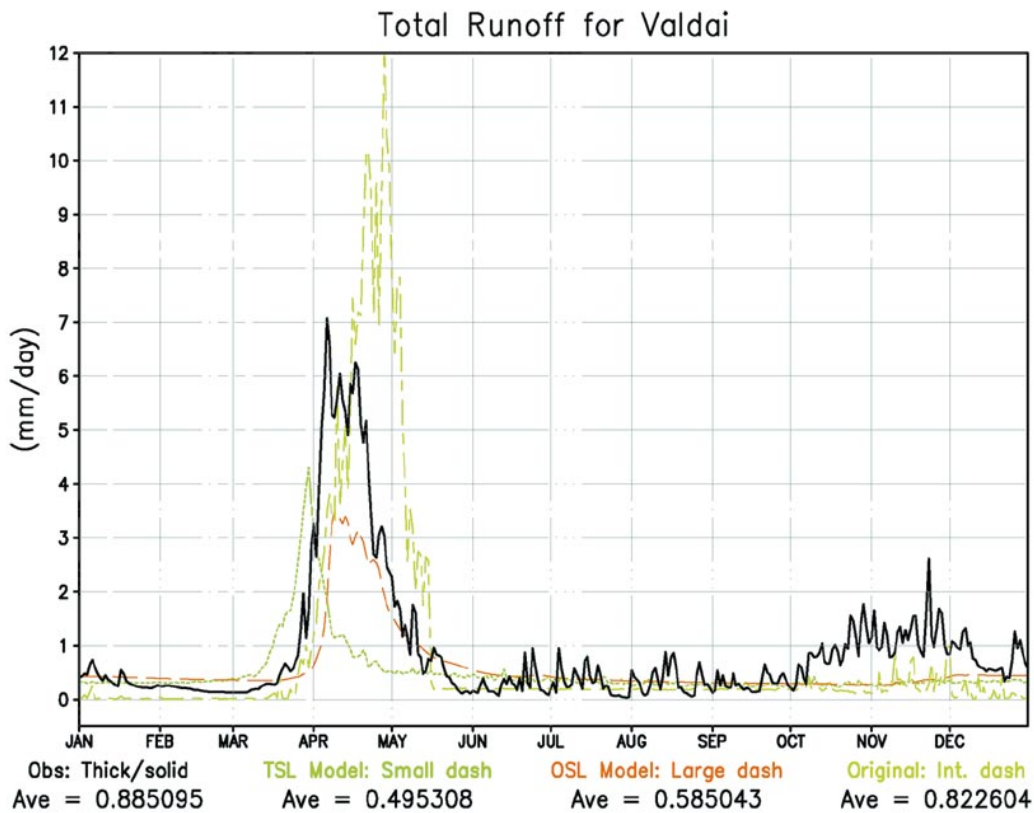


Figure 14. Same as in Figure 12, but for the total runoff (mm day^{-1}). The observed values are shown with a thin solid line.

The modifications to the calculation of evapotranspiration in this paper likely are not the root cause of the problem in this region, as the evapotranspiration from OSL and TSL differ only slightly during the summer. Other parameters such as incorrect vegetation and soil properties could also contribute to the error.

Figure 16 shows the annual cycle of simulated SSiB deep temperature T_d against the observed soil temperature at 80 cm below the surface. The original model, which had the coupled snow–soil layer, is unrealistically cold during the winter. TSL has the smallest annual amplitude of soil temperature that is in better agreement with observations. This suggests the addition of T_{dd} to an annual cycle of force–restore of the deep soil temperature is a useful modification.

5. Conclusions and discussion

Overall, the upgraded snow-physics package, along with other improvements to SSiB, have been shown to improve SSiB’s simulation of snow depth, meltwater infiltration, runoff, and soil temperatures. Both in the Russia Wheat Belt region and the Valdai simulation, the model’s improved physics lead to a better simulation

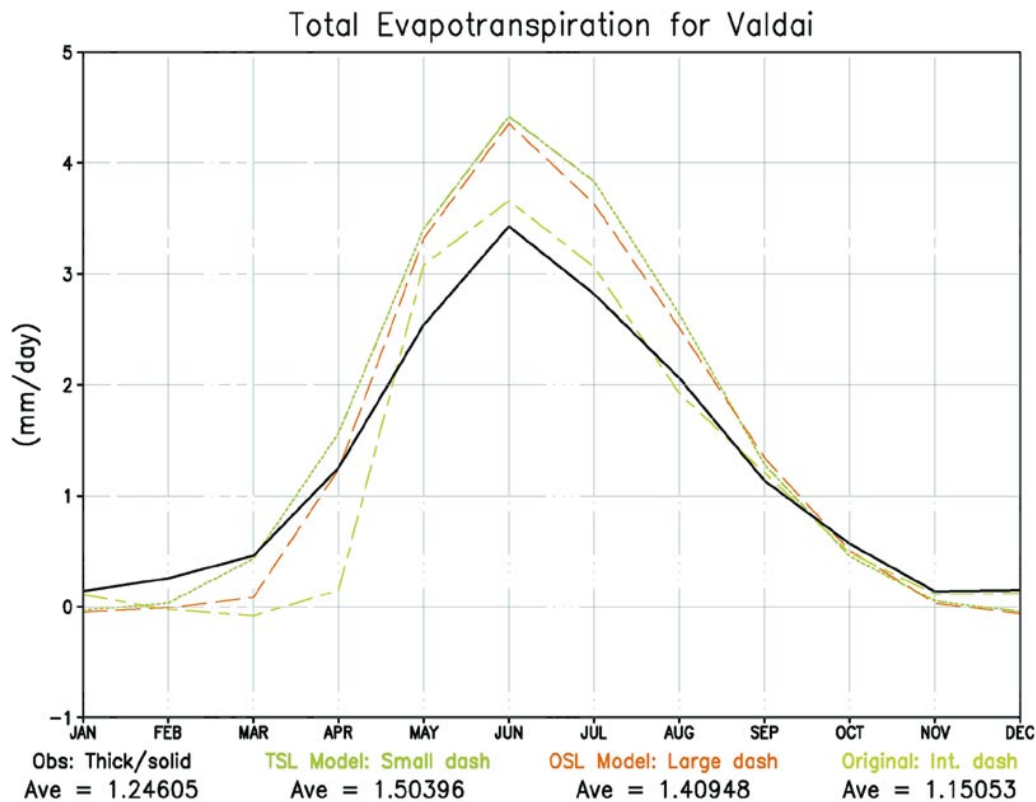


Figure 15. Same as in Figure 12 but for the total evapotranspiration in (mm day⁻¹).

of temperatures, which produces earlier snowpack melt and well-simulated soil moistures.

Some problems still remain, however. For example, the model may now be melting too early in some regions. The cause may be the lower snow albedo during melting periods. The snowmelt timing is also intimately related to diurnal snow layer properties and its thickness. Values taken for ρ_s , κ_p , and albedo, which are kept constant everywhere, deserve more attention (e.g., Loth and Graf, 1998b). Also, the values taken for T_{dd} have a large effect on the soil temperature under the snowpack and thus the initiation of snowmelt. The formulation of fractional snow cover and the effect of melting snow on albedo also seem to play an influential role, and better parameterizations for these processes need to be instituted. In addition, adding the effects of blowing snow (Liston and Sturm, 1998), solar absorption by snow on sloped surfaces, and subgrid snow cover effects (Liston, 1999) is expected to affect the simulation.

Additional multiyear validation datasets are needed to test the model. In addition to useful single-site datasets such as Valdai, longer time period global datasets would be useful to test the model at many different locations and periods. The upcoming GSWP 1.5 and GSWP 2 (using ISLSCP Initiative II data) projects are expected to lead

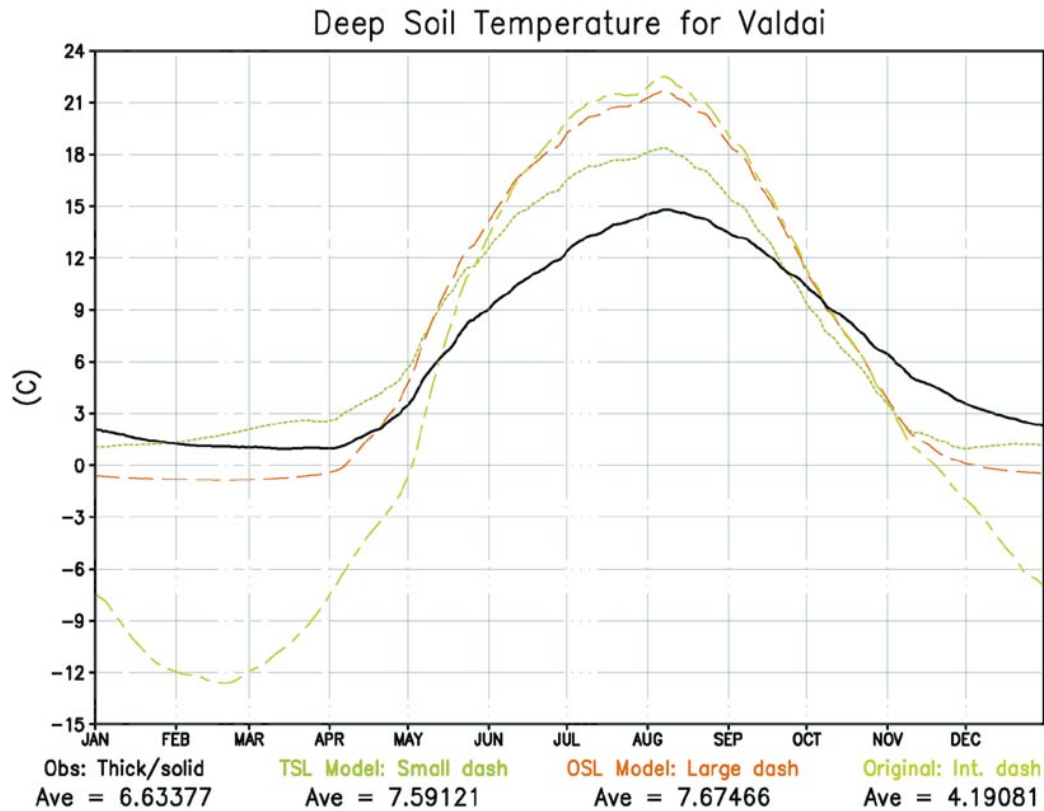


Figure 16. Same as in Figure 12 but for the deep soil temperature (°C).

to further opportunities to evaluation and improvement in SSiB's snow physics and hydrology.

SSiB has also been coupled to a very high resolution soil hydrology model for detailed soil moisture profiles. In its current form, 100 soil moisture layers of 5-cm thickness for a total depth of 5 m can be used within SSiB to improve simulation of the interlayer exchanges of water. Very often, the water table is above this 5-m depth; in such a case the water table interaction is explicitly resolved. A soil model such as this may lead to improved parameterizations in the three-layer SSiB and improve the simulation of evapotranspiration and baseflow.

Acknowledgments. The authors wish to thank Kenneth Bergman of NASA Headquarters and Rick Lawford of NOAA's Office of Global Programs for supporting this research. Thanks to Adam Schlosser for use of the PILPS 2(d) Valdai forcing data. Thanks also to Taikan Oki for discussions on the TRIP river routing model and to Joel Susskind for providing the TOVS Pathfinder A data. Thanks as well to Alan Robock, Steve Hollinger, and Konstantin Vinnikov for use of the soil moisture data. The GTOPO30 DEM data are distributed by the EROS Data Center Distributed Active Archive Center, located at the U.S. Geological Survey's EROS Data Center in

Sioux Falls, South Dakota. Streamflow data of major river basins, version 0, were provided by the Department of Hydrology and Water Resources, The University of Arizona, in cooperation with Dr. Wolfgang Grabs of the Global Runoff Data Center, Koblenz, Germany. NOAA Weekly Snow and Ice Cover Charts are produced and digitized by NOAA personnel. Quality control of the dataset, including limited adjustments to the files for standardization purposes, has subsequently been conducted at Rutgers University by Dr. David A. Robinson.

Appendix: Main Equations of the Snow-Physics Scheme

The prognostic equations for the three levels of the two-snow-layer model of SSiB (TSL) are described below. The subscripts used in this section refer to the layers as follows: sn is thin diurnal skin layer of snowpack, s is bulk snowpack layer, and d is blended soil and deep soil under snowpack. The prognostic equation for the diurnal, or top, snow layer is

$$C_{\text{sn}} \frac{\partial T_{\text{sn}}}{\partial t} = R_{n(\text{sn})} - H_{\text{sn}} - \lambda E_{\text{sn}} - \frac{2\pi C_{\text{sn}}}{\tau} (T_{\text{sn}} - T_s), \quad (\text{A1})$$

where C_{sn} is the effective heat capacity in joules per square meter per kelvin in $R_{n(\text{sn})}$ is the net radiation in watts per square meter, H_{sn} is the sensible heat flux in watts per square meter, λE_{sn} is the latent heat flux in watts per square meter (where λ is the latent heat of vaporization), and $\tau = 86\,400$ s. The sensible and latent heat fluxes are the same as used in Xue et al. [Xue et al., 1991, Eqs. (A5) and (A6)], except that T_{gs} and $e_{*(\text{gs})}$ are replaced by T_{sn} and $e_{*(\text{sn})}$.

The prognostic equation for the bulk snow layer is

$$C_s \frac{\partial T_s}{\partial t} = R_{n(s)} + \kappa_c (T_d - T_s) + \frac{2\pi C_{\text{sn}}}{\tau} (T_{\text{sn}} - T_s), \quad (\text{A2})$$

where C_s and $R_{n(s)}$ are the effective heat capacity in joules per square meter per kelvin and net radiation in watts per square meter of the bulk layer, and κ_c is the snow–soil interface conductivity in watts per square meter per kelvin (given later).

The prognostic equation for the blended soil and deep soil under the snowpack is

$$C_d \frac{\partial T_d}{\partial t} = R_{n(d)} - \kappa_c (T_d - T_s) + \frac{2\pi}{365\tau} (T_{\text{ad}} - T_d), \quad (\text{A3})$$

where C_d and $R_{n(d)}$ are the effective heat capacity of the soil and net radiation of the soil, respectively.

The net radiations in watts per square meter for all three levels with snowpack are

$$R_{n(\text{sn})} = \text{SW}_{\downarrow} (1 - \alpha) [1 - \exp(-\kappa_t Z_{\text{sn}})] + \text{LW}_{\downarrow} [1 - V_c (1 - \epsilon_c)] + \sigma_s T_c^4 V_c (1 - \epsilon_c) - \sigma_s T_{\text{sn}}^4, \quad (\text{A4})$$

$$R_{n(s)} = [\text{SW}_{\downarrow} (1 - \alpha) - R_{n(\text{sn})}] [1 - \exp(-\kappa_t Z_s)], \quad (\text{A5})$$

$$R_{n(d)} = \text{SW}_{\downarrow} (1 - \alpha) - R_{n(\text{sn})} - R_{n(s)}, \quad (\text{A6})$$

where $SW_{\downarrow}(1 - \alpha)$ is the sum of all four components (direct/diffuse, visible/near-IR) of the shortwave incident on the top of the snowpack and not reflected (α is the albedo) in watts per square meter, LW_{\downarrow} is the longwave incident on the top of the snowpack in watts per square meter, $Z_{sn} = 0.004$ m (4 mm) is the water equivalent depth of the diurnal snow layer, Z_s is the water equivalent depth in meters of the bulk snow layer, $\sigma_s = 8.76 \times 10^8 \text{ W m}^{-2} \text{ K}^{-4}$ is the Stefan–Boltzmann constant, T_c is the canopy temperature in kelvins, V_c is the fractional cover of the canopy vegetation, and ϵ_c is the dimensionless longwave emissivity. The transmittance coefficient for shortwave energy through the snow is $\kappa_t = 25.0$ per meter, which was incorrectly given as 23.0 per meter in Sud and Mocko [Sud and Mocko, 1999, Eq. (1)]. This value allows approximately 10% of the incoming absorbed/transmitted solar flux to pass through a 10-cm-thick snow/ice pack. The diurnal depth of 0.004 m water equivalent was used under the assumption that 10% of the incoming solar flux will be absorbed in the diurnal layer.

The blended conductivity of heat for the snow–soil interface, which conducts heat through the layers to the interface and radiates heat through a small assumed air gap between the layers, is

$$\kappa_c = \frac{1}{\left[\frac{0.5(1 + \sqrt{365})Z_1}{\kappa_d} + \frac{1}{4\sigma_s \left(\frac{T_s + T_d}{2} \right)^3} + \frac{0.5Z_s\rho_w}{\kappa_s\rho_s} \right]}, \quad (\text{A7})$$

where κ_d is the thermal conductivity of the soil in watts per meter per kelvin and κ_s is the thermal conductivity of snow in watts per meter per kelvin defined in Eq. (2).

The above equations are solved in a implicit backward method given in Sellers et al. (Sellers et al., 1986) and explained in more detail for use with snow physics in Sud and Mocko (Sud and Mocko, 1999). Other than the introduction of the very deep temperature equation [Eq. (6)], the prognostic equations for temperatures for snow-free land remain the same in SSIb due to Xue et al. (Xue et al., 1991).

References

- Alpert, P., Y. J. Kaufman, Y. Shay-El, D. Tanre, A. da Silva, S. Schubert, and J. H. Joseph, 1998: Quantification of dust-forced heating of the lower troposphere. *Nature*, **395**, 367–370.
- Chen, F., K. Mitchell, J. Schaake, Y. Xue, H.-L. Pan, V. Koren, Q. Y. Duan, M. Ek, and A. Betts, 1996: Modeling of land surface evaporation by four schemes and comparison with FIFE observations. *J. Geophys. Res.*, **101**(D3), 7251–7268.
- Chen, T. H., A. Henderson-Sellers, P. C. D. Milly, A. J. Pitman, A. C. M. Beljaars, J. Polcher, F. Abramopoulos, A. Boone, S. Chang, F. Chen, Y. Dai, C. E. Desborough, R. E. Dickinson, L. Dümenil, M. Ek, J. R. Garratt, N. Gedney, Y. M. Gusev, J. Kim, R. D. Koster, E. A. Kowalczyk, K. Laval, J. Lean, D. Lettenmaier, X. Liang, J.-F. Mahfouf, H.-T. Mengelkamp, K. E. Mitchell, O. N. Nasonova, J. Noilhan, A. Robock, C. Rosenzweig, J. Schaake, C. A. Schlosser, J.-P. Schulz, Y. Shao, A. B. Shmakin, D. L. Verseghy, P. Wetzell, E. F. Wood, Y.

- Xue, Z.-L. Yang, and Q. Zeng, 1997: Cabauw experimental results from the Project for Intercomparison of Land-surface Parameterization Schemes. *J. Clim.*, **10**, 1194–1215.
- Clapp, R. B., and G. M. Hornberger, 1978: Empirical equations for some soil hydraulic properties. *Water Resour. Res.*, **14**, 601–604.
- Deardorff, J. W., 1978: Efficient prediction of ground surface temperature and moisture, with inclusion of a layer of vegetation. *J. Geophys. Res.*, **83**(NC4), 1889–1903.
- Desborough, C. E., and A. J. Pitman, 1998: The BASE land surface model. *Global Planet. Change*, **19**, 3–18.
- Dirmeyer, P. A., A. J. Dolman, and N. Sato, 1999: The pilot phase of the Global Soil Wetness Project. *Bull. Am. Meteorol. Soc.*, **80**, 851–878.
- Douville, H. J.-F. Royer, and J.-F. Mahfouf, 1995: A new snow parameterization for the Météo France climate model. Part I: Validation in stand-alone experiments. *Clim. Dyn.*, **12**, 21–35.
- Henderson-Sellers, A., Z.-L. Yang, and R. E. Dickinson, 1993: The Project for Intercomparison of Land-surface Parameterization Schemes. *Bull. Am. Meteorol. Soc.*, **74**, 1335–1349.
- Hollinger, S. E., and S. A. Isard, 1994: A soil moisture climatology of Illinois. *J. Clim.*, **7**, 822–833.
- Jin, J. M., X. G. Gao, S. Sorooshian, Z.-L. Yang, R. Bales, R. E. Dickinson, S. F. Sun, and G. X. Wu, 1999: One-dimensional snow water and energy balance model for vegetated surfaces. *Hydrol. Processes*, **13**, 2467–2482.
- Liston, G. E., 1999: Interrelationships among snow distribution, snowmelt, and snow cover depletion: Implications for atmospheric, hydrologic, and ecologic modeling. *J. Appl. Meteorol.*, **38**, 1474–1487.
- Liston, G. E., and M. Sturm, 1998: A snow-transport model for complex terrain. *J. Glaciol.*, **44**, 498–516.
- Liston, G. E., Y. C. Sud, and E. F. Wood, 1994: Evaluating GCM land surface hydrology parameterizations by computing river discharges using a runoff routing model: Application to the Mississippi basin. *J. Appl. Meteorol.*, **33**, 394–405.
- Loth, B., and H.-F. Graf, 1998a: Modeling the snow cover in climate studies. 1. Long-term integrations under different climatic conditions using a multilayered snow-cover model. *J. Geophys. Res.*, **103**(D10), 11,313–11,327.
- Loth, B., and H.-F. Graf, 1998b: Modeling the snow cover in climate studies. 2. The sensitivity to internal snow parameters and interface processes. *J. Geophys. Res.*, **103**(D10), 11,329–11,340.
- Mahrt, L., and J. Sun, 1995: The subgrid velocity scale in the bulk aerodynamic relationship for spatially averaged scalar fluxes. *Mon. Weather Rev.*, **123**, 3032–3041.
- Meeson, B. W., F. E. Corprew, J. M. P. McManus, D. M. Myers, J. W. Closs, K.-J. Sun, D. J. Sunday, and P. J. Sellers, 1995: *ISLSCP Initiative I—Global Data Sets for Land–Atmosphere Models, 1987–1988*. Vols. 1–5. CD-ROM, NASA.
- Mocko, D. M., and Y. C. Sud, 1998: Comparison of a land-surface model (SSiB) to three parameterizations of evapotranspiration—A study based on ISLSCP Initiative I data. *Earth Interactions*, **2**. [Available online at <http://EarthInteractions.org>.]
- Mocko, D. M., G. K. Walker, and Y. C. Sud, 1999: New snow-physics to complement SSiB. Part II: Effects on soil moisture initialization and simulated surface fluxes, precipitation, and hydrology of GEOS II GCM. *J. Meteorol. Soc. Jpn.*, **77**, 49–366.
- Morrill, J. C., R. E. Dickinson, and A. N. Hahmann, 1999: Sensitivity of a land-surface model to the diurnal distribution of downward longwave radiation. *J. Meteor. Soc. Jpn.*, **77B**, 265–279.
- Oki, T., and Y. C. Sud, 1998: Design of Total Runoff Integrating Pathways (TRIP)—A global river channel network. *Earth Interactions*, **2**. [Available online at <http://EarthInteractions.org>.]
- Oki, T., T. Nishimura, and P. Dirmeyer, 1999: Assessment of annual runoff from land surface models using Total Runoff Integrating Pathways (TRIP). *J. Meteorol. Soc. Jpn.*, **77**, 235–255.

- Robock, A., K. Y. Vinnikov, C. A. Schlosser, N. A. Speranskaya, and Y. Xue, 1995: Use of midlatitude soil moisture and meteorological observations to validate soil moisture simulations with biosphere and bucket models. *J. Clim.*, **8**, 15–35.
- Sato, N., P. J. Sellers, D. A. Randall, E. K. Schneider, J. Shukla, J. L. Kinter, Y.-T. Hou, and E. Albertazzi, 1989: Implementing the Simple Biosphere Model (SiB) in a general circulation model: Methodologies and results. NASA Contractor Rep. 185509, 76 pp.
- Schlosser, C. A., A. Robock, K. Y. Vinnikov, N. A. Speranskaya, and Y. Xue, 1997: 18-year land-surface hydrology model simulations for a midlatitude grassland catchment in Valdai, Russia. *Mon. Weather Rev.*, **125**, 3279–3296.
- Schlosser, C. A., A. G. Slater, A. Robock, A. J. Pitman, K. Y. Vinnikov, A. Henderson-Sellers, N. A. Speranskaya, K. Mitchell, and the PILPS 2(d) Contributors, 2000: Simulations of a boreal grassland hydrology at Valdai, Russia: PILPS Phase 2(d). *Mon. Weather Rev.*, **128**, 301–321.
- Sellers, P. J., Y. Mintz, Y. C. Sud, and A. Dalcher, 1986: A Simple Biosphere model (SiB) for use within general circulation models. *J. Atmos. Sci.*, **43**, 505–531.
- Sellers, P. J., B. W. Meeson, J. Closs, J. Collatz, F. Corprew, D. Dazlich, F. G. Hall, Y. Kerr, R. D. Koster, S. Los, K. E. Mitchell, J. McManus, D. Myers, K.-J. Sun, and P. Try, 1995: An overview of the ISLSCP Initiative I global data sets. *ISLSCP Initiative I—Global Data Sets for Land–Atmosphere Models, 1987–1988*. Vol. 1, CD-ROM, NASA.
- Sellers, P. J., D. A. Randall, G. J. Collatz, J. A. Berry, C. B. Field, D. A. Dazlich, C. Zhang, G. D. Collelo, and L. Bounoua, 1996: A revised land surface parameterization (SiB2) for atmospheric GCMs. Part I: Model formulation. *J. Clim.*, **9**, 676–705.
- Slater, A. G., A. J. Pitman, and C. E. Desborough, 1998: The validation of a snow parameterization designed for use in general circulation models. *Int. J. Climatol.*, **18**, 595–617.
- Slater, A. G., C. A. Schlosser, C. E. Desborough, A. J. Pitman, A. Henderson-Sellers, A. Robock, K. Y. Vinnikov, K. Mitchell, A. Boone, H. Braden, F. Chen, P. M. Cox, P. de Rosnay, R. E. Dickinson, Y.-J. Dai, Q. Y. Duan, J. Entin, P. Etchevers, N. Gedney, Y. M. Gusev, F. Habets, J. Kim, V. Koren, E. Kowalczyk, O. N. Nasonova, J. Noilhan, J. Schaake, A. B. Shmakina, T. G. Smirnova, D. Verseghy, P. Wetzell, Y. Xue, Z.-L. Yang, and Q. Zeng, 2001: The representation of snow in land surface schemes: Results from PILPS 2(d). *J. Hydrometeorol.*, **2**, 7–25.
- Smirnova, T. G., J. M. Brown, S. G. Benjamin, and D. Kim, 2000: Parameterization of cold-season processes in the MAPS land-surface scheme. *J. Geophys. Res.*, **105**(D3), 4077–4086.
- Sud, Y. C., and D. M. Mocko, 1999: New snow-physics to complement SSiB. Part I: Design and evaluation with ISLSCP Initiative I datasets. *J. Meteorol. Soc. Jpn.*, **77**, 335–348.
- Sun, S. F., J. M. Jin, and Y. Xue, 1999: A simple snow–atmosphere–soil transfer model. *J. Geophys. Res.*, **104**(D16), 19,587–19,597.
- Susskind, J., P. Piraino, L. Rokke, L. Iredell, and A. Mehta, 1997: Characteristics of the TOVS Pathfinder Path A dataset. *Bull. Am. Meteorol. Soc.*, **78**, 1449–1472.
- Takacs, L. L., A. Molod, and T. Wang, 1994: Documentation of the Goddard Earth Observing System (GEOS) general circulation model—Version 1. NASA Tech. Memo. 104606, Vol. 1, 100 pp.
- Verseghy, D. L., 1991: CLASS—A Canadian Land Surface Scheme for GCMs. I. Soil model. *Int. J. Climatol.*, **11**, 111–133.
- Vinnikov, K. Y., and I. B. Yeserkepova, 1991: Soil moisture: Empirical data and model results. *J. Clim.*, **4**, 66–79.
- Vinnikov, K. Y., A. Robock, N. A. Speranskaya, and C. A. Schlosser, 1996: Scales of temporal and spatial variability of midlatitude soil moisture. *J. Geophys. Res.*, **101**(D3), 7163–7174.
- Xue, Y., 1997: Biosphere feedback on regional climate in tropical North Africa. *Q. J. R. Meteorol. Soc.*, **123**, 1483–1515.
- Xue, Y., P. J. Sellers, J. L. Kinter, and J. Shukla, 1991: A Simplified Biosphere model for global climate studies. *J. Clim.*, **4**, 345–364.

- Xue, Y., H. G. Bastable, P. A. Dirmeyer, and P. J. Sellers, 1996a: Sensitivity of simulated surface fluxes to changes in land surface parameterizations—A study using ABRACOS data. *J. Appl. Meteorol.*, **35**, 386–400.
- Xue, Y., F. J. Zeng, and C. A. Schlosser, 1996b: SSiB and its sensitivity to soil properties—A case study using HAPEX-Mobilhy data. *Global Planet. Change*, **13**, 183–194.
- Xue, Y., P. J. Sellers, F. J. Zeng, and C. A. Schlosser, 1997: Comments on “Use of midlatitude soil moisture and meteorological observations to validate soil moisture simulations with biosphere and bucket models.” *J. Clim.*, **10**, 374–376.
- Yang, Z.-L., R. E. Dickinson, A. Robock, and K. Y. Vinnikov, 1997: Validation of the snow submodel of the Biosphere–Atmosphere Transfer Scheme with Russian snow cover and meteorological observational data. *J. Clim.*, **10**, 353–373.
- Yen, Y., 1981: Review on thermal properties of snow, ice and sea ice. Special Rep. 81-10, Cold Regions Research and Engineering Laboratory, Hanover, NH, 35 pp.

Earth Interactions is published jointly by the American Meteorological Society, the American Geophysical Union, and the Association of American Geographers. Permission to use figures, tables, and *brief* excerpts from this journal in scientific and education works is hereby granted provided that the source is acknowledged. Any use of material in this journal that is determined to be “fair use” under Section 107 or that satisfies the conditions specified in Section 108 of the U.S. Copyright Law (17 USC, as revised by P.L. 94-553) does not require the publishers’ permission. For permission for any other form of copying, contact one of the copublishing societies.
